Templating an organic layer with the Si(111)-7 × 7 surface reconstruction using steric constraints

A. J. Weymouth,* G. J. A. Edge, and A. B. McLean†
Department of Physics, Engineering Physics & Astronomy, Queen's University, Kingston, Ontario, Canada K7L 3N6

R. H. Miwa
Instituto de Física, Universidade Federal de Uberlândia, C.P. 593, 38400-902 Uberlândia, Minas Gerais, Brazil

G. P. Srivastava
School of Physics, University of Exeter, Stocker Road, Exeter EX4 4QL, United Kingdom
(Received 11 June 2011; published 4 October 2011)

We demonstrate that the Si(111)-7 × 7 surface reconstruction can be used to template an ordered array of 1,3,5-methyl benzene molecules that are uniformly distributed over both the faulted and the unfaulted halves of the 7 × 7 unit cell by covalent attachment *in vacuo*. An intermolecular steric interaction, which hinders nearest-neighbor adsorption, is shown to play an important role in the formation of the ordered array. The stable equilibrium structure is shown to be one where the molecules are located at the corner of the half unit cells maximizing the intermolecular separation. In addition to the intermolecular steric interaction, there is an interaction between the molecule and the surface that plays a important role in reducing disorder in the array. Moreover, as the coverage is increased, there is a switch in site preference, from edge to corner, that mitigates the effect of the intermolecular interaction. To investigate this system we used scanning tunneling microscopy to study site occupancy as a function of coverage, *ab initio* total energy calculation to study the stability of the attachment sites, and Monte Carlo modeling to examine the emergence of translational order in the overlayer. The switch in site preference from edge to corner is faithfully reproduced by the kinetic Monte Carlo model when an interaction term is included.

DOI: 10.1103/PhysRevB.84.165308 PACS number(s): 68.43.Bc, 68.47.Fg, 68.37.Ef

I. INTRODUCTION

The successful manufacture of hybrid devices that utilize the optical response or the bio-functional properties of organic materials[1,2] faces the considerable challenge of interfacing the organic material to Si because crystalline Si is still used to manufacture the majority of microelectronic devices. Although a wide variety of ordered organic layers can be assembled on metal surfaces using surface-confined supramolecular coordination chemistry,[3,4] noncovalent synthesis is an inappropriate strategy for Si surfaces because Si surfaces are considerably more reactive.[5] This fact has prompted intense study of the organic-Si interface,[5–12] producing a much improved understanding of the physical factors at play during the initial stages of interface formation. However, there is a practical need to increase both the degree of order and the degree of selectivity in both organic mono- and multilayers grown on Si (Ref. 10).

Before attaching organic molecules to Si, one could passivate the surface with a substituent to reduce the reactivity. This has the additional benefit of making subsequent handling under ambient conditions possible.[5,9,13,14] Passivation is frequently adopted, for example, in wet-chemical and plasma-based processes. Alternatively, one could employ direct covalent attachment to the reconstructed Si surface *in vacuo*. These two approaches are complementary but in the latter, the possibility of direct covalent attachment to the dimers on Si(100)-2 × 1, or to the dangling bonds on Si(111)-7 × 7, is retained and this affords the possibility of templating layers with the symmetry of the surface reconstruction. Contrastingly, surface passivation frequently reduces the symmetry of the surface to that of the bulk.

On the Si(100)-2 × 1 surface, strategies for templating alkenes and dialkenes by direct covalent attachment *in vacuo* have existed for over a decade. A key development was the demonstration that cyclopentene[11,15] can be attached to the surface dimers by [2 + 2] cycloaddition. Despite the success of this approach on (100), it does not translate naturally to (111). Although Si dimers demarcate the 7 × 7 unit cell, they are fully coordinated. Consequently, on Si(111)-7 × 7, alternate attachment strategies have been explored.[12–14,16–20] Notwithstanding the success of these approaches, the challenge of finding room-temperature strategies for templating organic layers by direct covalent attachment to Si(111)-7 × 7, with the quality of cyclopentene/Si(100) and with equal occupancy of both the faulted and unfaulted 7 × 7 half cells, provides a significant challenge to our understanding of interface formation in this important system.

One obstacle to the formation of an ordered organic layer on 7 × 7 is the multiplicity of attachment sites that exist on the surface. In the 7 × 7 reconstruction, the dangling bonds located on the 6 rest atoms (Fig. 1; three are shown colored red in a half unit cell), the 12 adatoms (Fig. 1; six are shown colored blue), and the atom located in the corner hole (not shown) comprise a total of 19 reaction sites. The dangling bond on the Si adatoms is partially full with a nominal charge of $+\frac{7}{12}e$. The dangling bonds on both the rest atom and the atom in the corner hole are fully occupied with a nominal charge of $-e$. If alkenes or small aromatic molecules are adsorbed onto the 7 × 7 surface reconstruction, the preferred attachment mechanism is one where they bridge a Si rest atom and a neighboring Si adatom, forming two covalent bonds with the surface in a di-σ geometry.[10,21,22] Each Si rest atom is surrounded by three nearest-neighbor adatoms. Two of the adatoms are located at

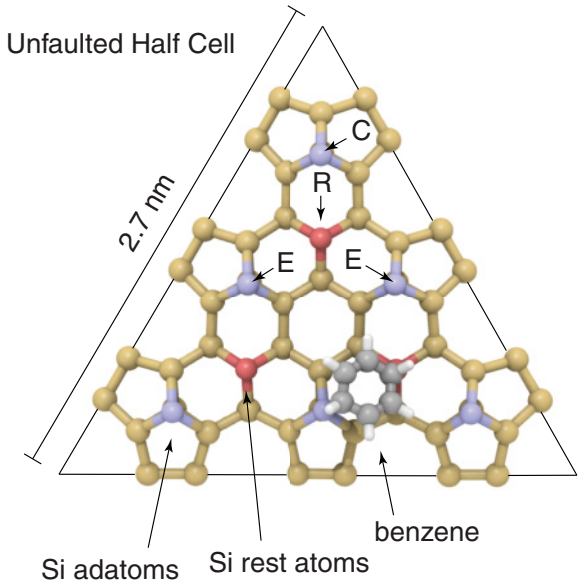

FIG. 1. (Color online) An admissible attachment geometry for a benzene molecule in the unfaulted half of the 7×7 unit cell bridging a Si rest atom (colored red) and a nearest-neighbor Si edge adatom (colored blue). Alternatively, the benzene molecule could bridge to the corner adatom located at the bottom-right corner or to the edge adatom location above and right. Similarly, there are three admissible bridging geometries for each of the other two rest atoms in the half cell.

the edge and one is located at the corner of the 7×7 half unit cell (HUC). The multiplicity of admissible attachment geometries leads to disorder. One possible geometry is illustrated in Fig. 1, where a benzene molecule is shown in a stable chemisorption geometry, bridging a rest atom and one of the nearest-neighbor edge adatoms. There are two other Si adatoms that represent possible bridges to this rest atom, one at the corner and one at the edge of the half cell.

In this paper, we demonstrate that steric hindrance can be used to induce order in the organic layer by introducing an energy penalty for nearest-neighbor adsorption. When nearest-neighbor adsorption is restricted in this fashion, the equivalence of the edge and corner adatom bridging sites is broken and the molecules favor the bridging sites that are located at the corner of the HUC because this maximizes their separation and minimizes their steric interaction. When molecules bind to edge sites, a Si adatom is actually imposed between each molecule. We illustrate this methodology with 1,3,5-methyl benzene (mesitylene) where the three methyl groups are responsible for the intermolecular steric interaction. Our approach builds upon a comparative study of methyl-benzene (toluene) and benzene adsorption on 7×7, where it was found that toluene had a greater preference for bridging sites located at the corner of the HUC than benzene.[23] Benzene's preferences for edge sites is commonly found for electron donors.[24] Toluene's increased preference for corner sites could not be explained in terms of electronegativity differences between benzene and toluene and it was, instead, attributed to steric interactions arising from toluene's additional methyl group.[23] Another reason for choosing mesitylene, rather than, for example, dimethyl benzene, is the fact that, due to its highly symmetric geometry, mesitylene provides a lower number of symmetrically distinct attachment geometries. This paper expands upon an earlier work where we first reported the possibility of assembling arrays using this approach.[25]

II. METHODS

A. Scanning tunneling microscopy

The adsorption of mesitylene on 7×7 was studied using scanning tunneling microscopy (STM) in an ultrahigh-vacuum (UHV) chamber with a base pressure of 5×10^{-11} Torr. The 7×7 surface was prepared by resistively heating 5×15-mm (111) samples (Virginia Semiconductor Inc., USA) to $\approx$1250 °C with ac current for 40 s, annealing it at 850 °C for 120 s and subsequently cooling it at a rate of 1 °C/s. All sample temperatures were verified with an infrared pyrometer. Mesitylene (Sigma-Aldrich, USA) was obtained in liquid form (>99%) and purified using seven freeze-pump-thaw cycles until no gas evolution could be observed. Once purified, it was leaked into the UHV chamber via a precision leak valve in the gas phase.

B. Density functional theory

The calculations were performed in the framework of the density functional theory (DFT),[26] using the generalized gradient approximation due to Perdew, Burke, and Ernzerhof.[27] The electron-ion interaction was treated by using norm-conserving fully separable pseudopotentials.[28,29] The Kohn-Sham (KS) wave functions were expanded in a combination of pseudoatomic numerical orbitals.[30] Essentially a double-ζ basis set, including polarization functions (*DZP*), was employed to describe the valence electrons.[31] The self-consistent total charge density was obtained by using the SIESTA code.[32] The 7×7 surface was simulated using the periodic slab method, with a supercell containing six monolayers of Si with a 7×7 surface unit cell plus a vacuum region of $\sim$12 Å. An energy cutoff of 120 Ry was used for the reciprocal-space expansion of the total charge density, and the Brillouin zone was sampled by using one special **k** point. Two hundred ninety-eight Si atoms were used and, in the bottom layer, 49 dangling bonds were saturated with hydrogen atoms. The convergence of the results was verified with respect to the number and choice of the special **k** points using up to four **k** points. Some results for binding energy and equilibrium geometry were further checked by (i) using a plane wave basis set with an energy cutoff of 25 Ry and and a cutoff of 100 Ry for wave functions and total charge density and (ii) including van der Waals interaction (vdW-DFT), within a semiempirical approach,[33] as implemented in the SIESTA code.[32] Equilibrium geometries were obtained by full relaxation of atoms in the four topmost Si layers and the adsorbed molecule. A force convergence criterion of 20 meV/Å was used.

C. Kinetic Monte Carlo model

The kinetic Monte Carlo (KMC) model that we used to study the assembly of the ordered molecular array evolved from a previous model that we successfully used to study thiophene adsorption on 7×7.[34] In the model, molecules may reside in either a chemisorbed or a mobile precursor

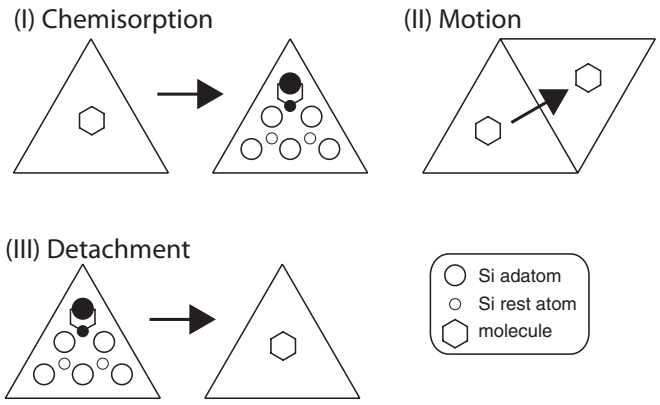

FIG. 2. Schematic representation of the three processes allowed in the KMC model. (I) A physisorbed molecule can chemisorb to an available adatom-rest atom pair in the HUC it is above, thus saturating the participating adatom and rest atom (as illustrated by their shading). (II) A physisorbed molecule can move to a neighboring HUC. (III) A chemisorbed molecule can detach, returning to the physisorbed state.

(physisorbed) state. The location of the molecules is taken to be the HUC within which the molecule resides, and molecular motion within the HUC is ignored. Consequently, molecules in the mobile precursor state are considered to be resident over a particular HUC and move by hopping to adjacent HUCs. Chemisorbed molecules are confined to a particular HUC, and the adatom-rest atom pair to which they attach is recorded. It is essential to do this because chemisorption eliminates reaction centers and restricts subsequent chemisorption. In the simulation, molecules may transfer from the physisorbed state to the chemisorbed state and *vice versa*. These processes occur at different rates because different activation energies are involved. Periodic boundary conditions were used for the surface, and simulations performed with different surface sizes indicated that using 32×16 HUCs was sufficient to produce convergence of the numerical results.

Our model admits the following three processes (see Fig. 2).

(I) A molecule in the mobile precursor (physisorbed) state overcomes an activation energy barrier and enters a chemisorption state located within the same HUC. This is a thermally activated process,[35] described by an Arrhenius relationship $\nu_{c,s} = \nu_o \exp(-E_s/k_B T)$, where $\nu_{c,s}$ represents the rate of chemisorption above site s, E_s is the associated energy activation barrier of that site, $k_B T$ is the thermal energy, and ν_o is the frequency prefactor, taken to be 10^{10} Hz.[36]

(II) A molecule in the mobile precursor (physisorbed) state moves to one of the neighboring three HUCs. The rate associated with this process was assumed to be $\nu_p = 0.01\nu_o$. Consequently, at room temperature, with $E_s \approx 0.2$ eV, $\nu_c \approx 0.4\nu_p$. A study of benzene on 7×7 found that physisorbed molecules avoided HUCs which contain chemisorbed molecules.[35] To reproduce this effect, the rate of physisorbed movement was made to depend upon the number of chemisorbed molecules in the destination HUC by reducing the rate by 25% for each chemisorbed molecule in the destination HUC. The reduction of 25% was specifically chosen because it prevented physisorbed molecules from becoming trapped if all nearest-neighbor HUCs were saturated.

(III) A chemisorbed molecule overcomes an activation energy barrier and re-enters the mobile precursor (physisorbed) state within the same HUC. In this simulation, the rate at which molecules were able to detach from the surface and reenter the physisorbed state (ν_d) was treated as an unknown and assumed to be site-independant (see later).

D. Results

1. Scanning tunneling microscopy

Four panels of Fig. 3, e.g., panels (d)–(g), illustrate the emergence of order, specificallly the formation of a mesitylene array as molecules are progressively added to the surface. The average mesitylene coverage in Fig. 3(d) is 0.11 molecules/7×7 cell corresponding to $\approx$2% of the saturation coverage. A single 7×7 cell has been highlighted in panel (d) and in the lower half of the unit cell there is what appears to be a missing edge adatom. The dark feature is the signature (see next section), shared by many other small organic molecules, of chemisorption on 7×7. In this particular case, the molecule bridges the adatom located at the edge of the HUC and the adjacent rest atom removing state density from the energy range accessible to the tunneling electrons. In Fig. 3(e), the average mesitylene coverage is 1.26 molecules/7×7 cell or $\approx$21% of the saturation coverage. A unit cell has once again been highlighted in which all Si adatoms are visible. However, in neighboring unit cells one can see evidence for mesitylene adsorption in both corner and edge sites. In Fig. 3(f), the average mesitylene coverage is 5.34 molecules/7×7 cell or $\approx$89% of the saturation coverage. At this coverage the image is dominated by edge adatoms. A unit cell has been highlighted in Fig. 3(f) and in this cell all corner adatoms are suppressed, indicating the presence of six mesitylene molecules in corner sites. At the saturation coverage of six molecules/unit cell [Fig. 3(g)] the image is dominated by the edge Si adatoms that *do not* form covalent bonds with the mesitylene molecules.

From image sequences, such as the ones presented in Fig. 3, the average occupancy of each site as a function of coverage can be extracted. This was done for the bridging sites that involved the following four adatom types: faulted edge, faulted corner, unfaulted edge, and unfaulted corner. This information is presented later in Fig. 13. To generate Fig. 13, more than 3000 chemisorption sites were counted at six different mesitylene coverages. A study of site occupation as a function of coverage reveals that at coverages below two molecules per 7×7 cell, mesitylene shows a preference for bridging sites located at the edge of the unit cell. Two molecules/7×7 cell is $\frac{1}{3}$ of the saturation coverage and, alternatively, it represents one molecule per HUC. (The saturation coverage of one molecule per rest atom implicates the rest atoms in the formation of the Si-mesitylene covalent bond.) The unit cell that has been highlighted in Fig. 3(d), for example, contains a single mesitylene molecule that is bridging a Si rest atom and a Si edge adatom located in the lower right hand side of the 7×7 cell. As the coverage is increased above two molecules per 7×7 cell, the site preference switches and a preference for corner sites is maintained until the saturation coverage. Our experimental studies have also revealed that other small aromatic molecules such as benzene and thiophene, that also

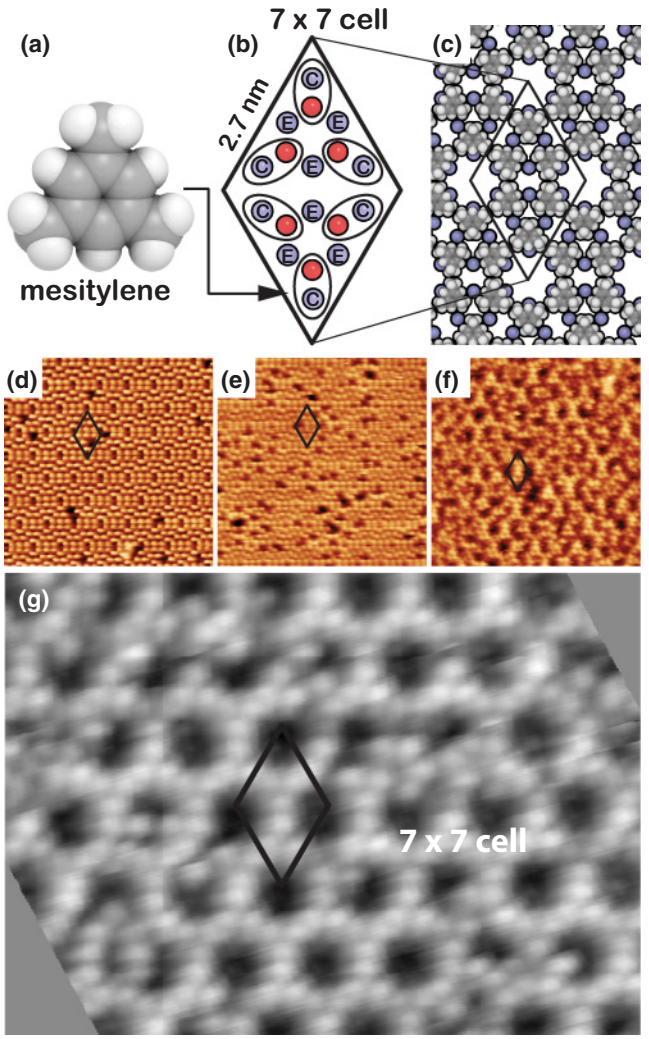

FIG. 3. (Color online) (a) At saturation, six 1,3,5-methyl benzene (mesitylene) molecules, shown in space-filling representation, are located within the 7×7 cell at the positions defined by the ellipses (see later). Each molecule bridges a rest atom/corner adatom pair. (b) The adatoms (rest atoms) are colored blue (red). The edge (E) and corner (C) adatoms are labeled and the unit cell has side 2.7 nm. (d) STM data of 7×7 with an average coverages of 0.11 (e) 1.26 and (f) 5.34 and (g) 6.00 molecules/unit cell; 19×19 nm, -0.8 V, 0.6 nA. The bright features in the image correspond to the location of the Si adatoms (blue) that *are not* involved in covalent bond formation with mesitylene molecules.

attach to the surface in a di-σ geometry, do not reverse their site preference as the coverage is increased. Instead, they both show a preference for edge adatoms that is preserved throughout the entire coverage range right up to saturation. Mesitylene is, therefore, different and this difference, we argue, suggests the presence of an additional intermolecular interaction for mesitylene that becomes important when more than two molecules are placed within a 7×7 cell. The origins of this interaction are examined in the next section.

Another striking property of the mestiylene/7×7 system is the lack of preference for either unit cell. This is illustrated quantitively in Fig. 13 (see later). We find that the molecule attaches to either HUC with equal probability. For organic molecules on 7×7 this behavior is uncommon but if an ordered structure is to be assembled with an equal occupancy of both faulted and unfaulted half cells, clearly it is a necessary property. This adsorption behavior can be contrasted with the interesting behavior of zwitterionic molecules, that can also be patterned by the 7×7 surface reconstruction. However, in the case of patterns with translational periodicity, the electrostatic interaction between the molecule and the surface leads to a preferential occupancy of the faulted half cell at saturation coverage.[20] This preference is normally explained using the concept of local softness: the ability of the 7×7 surface states to accept/donate charge.[24]

2. *Density functional theory*

Single-molecule adsorption geometries. Before studying the array structures that occur near saturation coverage, the energetic stability, the equilibrium geometry, and the electronic properties of single molecules on the 7×7 surface reconstruction were investigated. Specifically, we considered the bridging geometries, where the molecule attaches to the surface by [4 + 2] cycloaddition. In this geometry, two carbon atoms in the C_6 ring, located opposite one another, form covalent bonds (di-σ) with the surface [Figs. 4(a)–4(e)]. Similar to other small aromatic molecules, for example, benzene,[35,37–41] toluene,[41] and thiophene,[34,42–44] mesitylene bridges a rest atom and a neighboring adatom in the 7×7 reconstruction. This geometry is supported by a comparison of experimental and

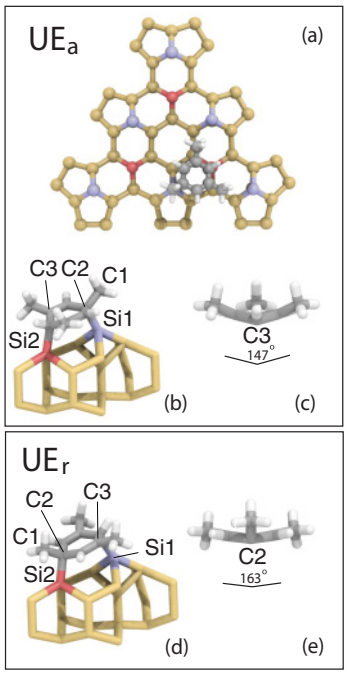

FIG. 4. (Color online) Equilibrium geometry of the adsorbed mesitylene molecule in (a)–(c) the UE_a (unstable) and (d),(e) UE_r (stable) bridging geometries; see the text. In panels (c) and (e) the surface has been removed to clearly show the distortion of the C_6 ring that is produced by the repulsive interaction between the methyl groups and the surface. The proximity of the two methyl groups to the Si surface is illustrated in panel (a) and the representation of the models has been modified to make the distortion of the C_6 ring clearer.

simulated STM images (see later) and it is consistent with the fact that the saturation coverage corresponded to one molecule per Si rest atom. However, unlike benzene, the C_3 rotational symmetry of mesitylene admits two inequivalent adsorption geometries. One of these has the carbon atom that is attached to the methyl group bonded to a Si rest atom; the other has the carbon atom that is attached to the methyl group bonded to a Si adatom. These geometries are described by the labels *r* and *a*, respectively, and they are illustrated in Figs. 4(a)–4(e). Additionally, the edge (E) and corner (C) adatoms located in each HUC are inequivalent. Therefore, there are a total of eight distinct bridging configurations: four in the faulted (F) and four in the unfaulted (U) HUC. To describe these configurations we use the following notation. The configuration shown in Figs. 4(d) and 4(e) is labeled UE_r because it is located in the unfaulted (U) half of the unit cell, bridging a rest atom and an edge (E) adatom with the methyl group above the rest atom (r). By rotating the molecule by 60°, the UE_a bridging configuration is created. The complete set of bridging geometries is, therefore, FE_r, FE_a, FC_r, FC_a, UE_r, UE_a, UC_r, and UC_a.

In general, the mesitylene adsorption energy (E_{ads}) can be calculated using

$$E_{\text{ads}} = E[\text{Si}(7\times7)] + nE[\text{mesitylene}] - E[\text{mesitylene/Si}(7\times7)] - \delta_{\text{BSSE}}, \quad (1)$$

where $E[\text{Si}(7\times7)]$ is the total energy of the isolated 7×7 surface, $E[\text{mesitylene}]$ is the total energy of an isolated mesitylene molecule, $E[\text{mesitylene/Si}(7\times7)]$ is the total energy of the combined system, and n is the number of mesitylene molecules that are added to each 7×7 cell. The last term, δ_{BSSE}, has been included to correct the basis set superposition error (BSSE).[45,46] Within our calculation approach the KS wave functions were expanded in a basis set composed of pseudoatomic orbitals; thus, in the first three terms of E_{ads} we are comparing total energies with different basis sets, which is corrected by including δ_{BSSE}.

Table I summarizes the calculated adsorption energies for a single mesitylene molecule [$n = 1$ in Eq. (1)] on the 7×7 surface in each of the eight bridging sites. For the energetically most stable geometry located in the unfaulted HUC and in an edge-bridging site, UE_r, we find that mesitylene adsorption is an exothermic process and at low coverage and in thermodynamic equilibrium, a preference for edge sites over corner sites and also a preference for the unfaulted half cell over the faulted half cell is expected. Specifically, in the unfaulted half of the unit cell, adsorption at the edge site (UE_r) is more favorable than adsorption at the corner site (UC_r) by 38 meV. In the faulted half of the unit cell, adsorption at the edge site (FE_r) is more favorable than adsorption at the corner site (FC_r) by 30 meV. Moreover, UE_r is energetically more favorable than FE_r by 25 meV and UC_r is energetically more favorable than FC_r by 17 meV.

In the E_a and C_a configurations [Fig. 4(b)], the mesitylene molecule is rotated by 60° with respect to E_r and C_r [Fig. 4(a)]. The calculated adsorption energies indicate that the E_a and C_a geometries are unlikely to be stable chemisorption geometries at room temperature. This is because when compared with their E_r and C_r counterparts (Table I), their absorption energies are lower by 0.4–0.5 eV. This has important consequences for the amount of disorder in the organic layer, to be discussed later.

Molecular adsorption on surfaces is affected by van der Waals (vdW) interaction. To investigate the effect that this interaction has on the single-molecule adsorption energies we recalculate the binding energies using the vdW-DFT scheme, described above. It was found that the unfaulted edge (UE_r) configuration remained the preferred single-molecule adsorption configuration. Specifically, the total energy difference between the unfaulted edge (UE_r) and the unfaulted corner (UC_r) configuration increased slightly from 38 meV (see Table I) to 42 meV. The binding energy difference between the preferred UE_r configuration and the rotated configuration UE_a, which we argued above was unstable, also increased from 0.44 to 0.52 eV. This comparison suggests that the DFT values, listed in Table I, are a reliable guide to the equilibrium configurations of this system. This conclusion is support by the fact that the vdW-DFT Si-C bond lengths were also found to be within 1% of the DFT Si-C bond lengths; the vdW interaction has only a minor effect on the adsorption configurations.

The energetic stability of the E_r and C_r geometries is related to the smaller structural deformation of the C_6 ring, as shown in Figs. 4(c) and 4(e). The distortion of the C_6 ring is considerably larger for the E_a and C_a structures and this arises from the repulsive interaction between the two CH_3 groups located close to the Si surface and the Si surface. The total energies of the isolated molecules were compared while retaining their adsorption geometries as depicted in Fig. 4. We found that the total energy of the *a* configuration is higher by ∼0.16 eV and from this we can conclude that the deformation of the adsorbed molecule does play an important role in destabilizing the *a* geometry relative to the *r* geometry. The bond lengths are also affected by the repulsive interaction between the adsorbed molecule and the surface. As presented in Table II, the C3-Si2 bonds for UE_a [Fig. 4(b)] are stretched by ∼0.08 Å compared with the C2-Si2 bonds for UE_r [Fig. 4(d)].

We have argued that the repulsive interaction between the mesitylene methyl groups and the surface reduces the

TABLE I. Calculated adsorption energies, E_{ads}, for the eight bridging geometries in units of eV/molecule, calculated using the procedure described in the text.

Unfaulted HUC	E_{ads}	Faulted HUC	E_{ads}
UE_r	0.687	FE_r	0.662
UC_r	0.649	FC_r	0.632
UE_a	0.246	FE_a	0.148
UC_a	0.238	FC_a	0.167

TABLE II. C-Si equilibrium bond lengths in Å. Si1 (Si2) denotes the adatom (rest-atom).

Unfaulted HUC	C-Si1	C-Si2	Faulted HUC	C-Si1	C-Si2
UE_r	2.03	2.03	FE_r	2.03	2.04
UC_r	2.02	2.03	FC_r	2.03	2.04
UE_a	2.00	2.08	FE_a	2.00	2.09
UC_a	2.00	2.06	FC_a	2.00	2.08

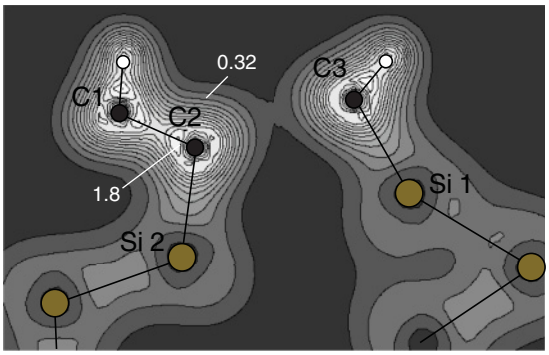

FIG. 5. (Color online) Total charge density for the UE_r bridging configuration, located in the unfaulted half of the unit cell and involving an edge adatom, shown along the C2-Si2 and C3-Si1 bonds (see Fig. 4). The contours are in units of 0.1 $e/(\text{a.u.})^3$.

adsorption energy of the molecule. In order to provide further support for this statement, we examined the adsorption of benzene on 7 × 7. In this case, of course, there are no methyl groups. Using the calculational approach that we introduced earlier, we find adsorption energies of 0.739 and 0.722 eV for the UE and the FE configurations, respectively. These are both larger than the calculated adsorption energies for mesitylene (Table I). Comparing the strain energies, it is found to be 1.95 eV/molecule for adsorbed benzene and 2.16 eV/molecule for adsorbed mesitylene. Consequently, the strain induced in the benzene is lower by 0.21 eV/molecule because the interaction with the surface does not produce a commensurate distortion of the C_6 ring.

The results presented in Table I indicate that for single mesitylene adsorbates, edge sites are more stable than corner sites: Specifically, E_r is more stable than C_r. The detailed nature of the electronic interaction between the molecule and the surface that leads to C-Si covalent bonds is clearly very important. Figure 5 contains a charge density plot that illustrates the formation of the C-Si chemical bonds between mesitylene, located in the stable UE_r bridging configuration, and the Si surface. Similar total charge densities have been found for the other E_r and C_r bridging geometries. As expected, most of the charge density moves toward the more electronegative C atoms. The strength of the C-Si chemical bonds can be inferred from the electronic states associated with the different bridging geometries. This is done using the average binding energies for the two stable bridging geometries, UE_r and UC_r,

$$\bar{\varepsilon} = \frac{\int_{\infty}^{E_F} \varepsilon g(\varepsilon) d\varepsilon}{\int_{\infty}^{E_F} g(\varepsilon) d\varepsilon}, \tag{2}$$

where ε represents the calculated (self-consistent) single-particle energy level and $g(\varepsilon)$ the respective density of states. For each bridging geometry, we calculated $\bar{\varepsilon}$ using the Si and C electronic states that are involved in the C-Si bonds. We found that the occupied electronic states of UE_r are more tightly bonded than those for UC_r by 0.14 eV. Calculations of this sort also demonstrate that the unfaulted HUC is preferred in thermodynamic equilibrium; UE_r is more stable than FE_r in accordance with our calculated adsorption energies (see Table I).

The total density of states (DOS) for the mesitylene/7 × 7 system in UE_r bridging geometry, and also the projected DOS (PDOS) for the molecule, is presented in Fig. 6(a). These results clearly show that the electronic contribution from the adsorbed molecule is almost negligible within $E_F \pm 1$ eV; the majority of the electronic states associated with the molecule actually lie between 3.5 and 7 eV below E_F. Figures 6(b) and 6(c) present the PDOS of the Si rest atom and the Si adatom, respectively. In those figures, the solid (dashed) lines represent the PDOS after (before) the formation of C-Si chemical bonds. The suppression of the electronic states near the Fermi level [dashed → solid lines in Figs. 6(b) and 6(c)] indicates that the Si dangling bonds are saturated upon mesitylene adsorption. The PDOS calculations suggest that the electronic states of the molecule and the electronic states of the Si rest atom and the Si adatom, which form covalent bonds with the molecule, will be weakly detected in STM topographical images with typical experimental values. We verified this by calculating STM image simulations using the Tersoff-Hamman approach.[47] Figures 7(a) and 8(a) are the

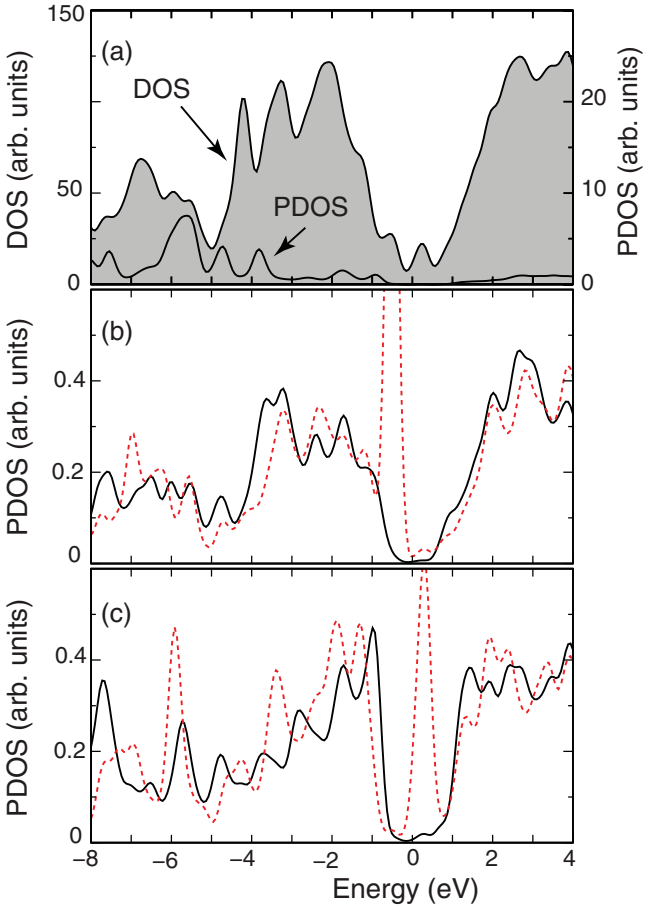

FIG. 6. (Color online) (a) The calculated DOS for the UE_r structure is shown shaded as is the PDOS of chemisorbed mesitylene. (b) The PDOS of the Si rest atom; Si2 in Fig. 4. (c) The PDOS of the Si adatom; Si1 in Fig. 4. In both (b) and (c) the dashed red line indicates the PDOS before the formation of C-Si chemical bonds and the solid black line indicates the PDOS after the formation of C-Si chemical bonds. In all panels, zero energy corresponds to the Fermi energy.

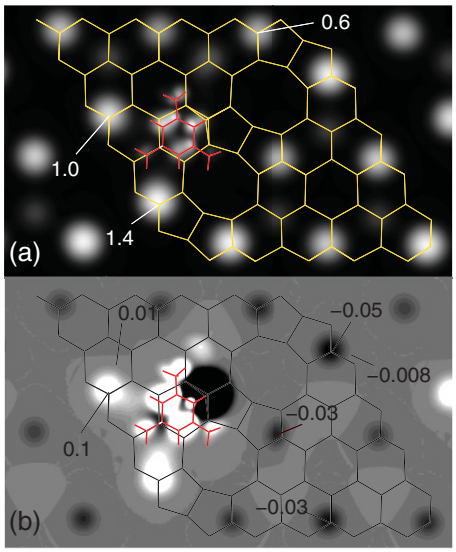

FIG. 7. (Color online) (a) Simulated STM image and (b) averated partial charge transfers calculated above the Si adatoms in the range, 2.0–4.0 Å. The molecule was located in the UE_r bridging geometry. In this geometry the carbon atom that forms a covalent bond with the Si rest atom also is attached to a methyl group. Occupied states within the energy range E_F–0.5 eV were used in the simulated image, a typical experimental value. In (b), bright (dark) regions indicate an increase (reduction) of the electronic charge density. The numerical values on the figures are in units of 10^{-4} e/a.u.^{3}

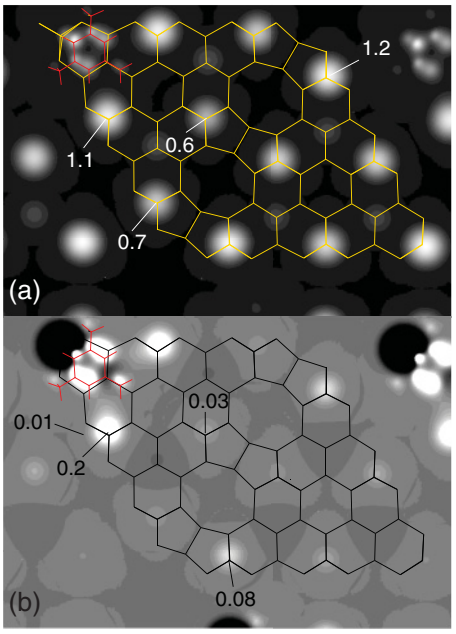

FIG. 8. (Color online) (a) Simulated STM images and (b) averaged partial charge transfers for mesitylene in the UC_r bridging geometry. A spatial range of 2.0–4.0 Å above the Si adatoms and an energy range of E_F–0.5 eV (occupied states) was used. In (b), bright (dark) regions indicate an increase (reduction) of the electronic charge density. The numerical values on the figures are in units of 10^{-4} e/a.u.^{3}

simulated STM images of mesitylene in the UE_r and UC_r bridging geometries, respectively. For both geometries we considered an energy window of 0.5 eV below the Fermi level, sampling electronic states located 2.0–4.0 Å above the topmost Si adatom. The brightest features in the simulated images are coincident with the Si adatoms, and in accordance with the PDOS calculations, the electronic contributions from the mesitylene adsorption sites are relatively small. Additionally, in the UE_r bridging configuration, it is noticeable that the corner and edge Si adatoms, located nearest the mesitylene adsorption site, are brighter, while the nearest-neighbor edge adatom, located on the faulted HUC, becomes darker than the other adatoms [Fig. 7(a)]. It is also clear from the simulation that the C atoms that are not forming σ bonds with the Si adatom/rest atoms appear brightest. The C-C bond lengths in the isolated molecule are 1.41 Å. However, for the adsorbed molecule, the bond lengths of the C atoms that appear bright is reduced to 1.38 Å, whereas the other four C-C bonds are elongated to 1.51–1.52 Å.

In Fig. 8(a) corresponding results are presented for the UC_r bridging geometry. In this configuration, the mirror symmetry of the 7×7 unit cell is preserved. When a comparison is made with the other Si adatoms in the unit cell, the nearest-neighbor edge adatoms become brighter, whereas the nearest-neighbor corner adatoms darken. The mirror plane is perpendicular to the plane of the surface and it also intersects the molecules and the corner adatom that is furthest from the molecule (the long diagonal of the unit cell).

Atomic relaxations, induced by the adsorption of the molecule, can of course contribute to the features observed for the UE_r and UC_r configurations. However, we find that the induced atomic displacements in both UE_r and UC_r bridging geometries are very small, with vertical displacements (of Si adatoms) smaller than 0.07 Å. Similar to the adsorption of benzene on Si(111),[48] our results suggest that in the STM images, *the changes in intensity are primarily due to modification to the electronic structure of the surface*.

The adsorption-induced changes in the surface's electronic structure can be studied by comparing the electronic charge density (DOS) for (i) the reacted mesitylene/7×7 system with the mesitylene molecule removed and (ii) the reacted mesitylene/7×7 system. Because the Si atoms are in the same position in both cases, the difference will provide information about charge transfer. The comparison is performed using an energy range of 0.5 eV located below the Fermi level, the energy range used in the STM simulations. Figure 7(b) shows how the occupied electronic states for the UE_r configuration are modified. Notably, the DOS associated with the Si adatoms located nearest the adsorbed molecule, specifically one edge and one corner adatom in the unfaulted HUC, increases. In contrast, the DOS associated with the other Si adatoms is reduced. Even those Si adatoms located in the faulted HUC show a DOS reduction. The corner adatoms in the faulted half look bright. These changes in electronic structure are not localized: The entire 7×7 cell is affected. In contrast, the charge transfers associated with the UC_r bridging geometry are more localized. As can be seen in Fig. 8(b), there is an increase in the electronic charge density on the nearest-neighbor edge Si adatoms in the unfaulted HUC, as well as on the corner Si adatoms of the faulted HUC.

Adsorption geometries involving more than one mesitylene molecule per 7×7 cell. So far, we have described the

TABLE III. Calculated adsorption energies E_{ads} for two molecule adsorption geometries in units of eV/molecule.

Geometry	E_{ads}	Geometry	E_{ads}
UC_rFC_r	0.667	FE_rFC_r	0.600
UC_rUC_r	0.665	FE_rFC_a	0.409
FC_rFC_r	0.645	UC_rFC_a	0.454

adsorption of single mesitylene molecules on the 7 × 7 cell. However, to study the interaction between adsorbed molecules we need to study adsorption geometries with more than one molecule per 7 × 7 cell. In Table III, we present adsorption energies calculated using two molecule adsorption geometries. These geometries have been described using the notation introduced earlier for single molecular adsorption.

As can been seen from Table III, there are two energetically equivalent configurations: UC_rFC_r and UC_rUC_r. In the former there are two molecules in corner sites: One is located in the unfaulted and the other is located in the faulted HUC. The adsorption energy for this geometry is E_{ads} = 0.667 eV/molecule. In UC_rUC_r there are two molecules in corner sites. Both are located in the unfaulted HUC and the adsorption energy is 0.665 eV/molecule. The slight energetic preference for the adsorption on the unfaulted HUC has been maintained, with the formation of two mesitylene molecules on the faulted HUC (the FC_rFC_r configuration; see Fig. 9) being energetically less stable by 20 meV/molecule when compared with UC_rUC_r. Due to the lateral separation between the adsorbed mesitylene molecules, the formation of E_rC_r pairs within the same HUC is energetically less stable than C_rC_r pairs. For example, the adsorption energy of FE_rFC_r is lower by 67 meV/molecule than UC_rFC_r. Similar repulsive interaction is present when two molecules are located at edge sites within the same HUC.

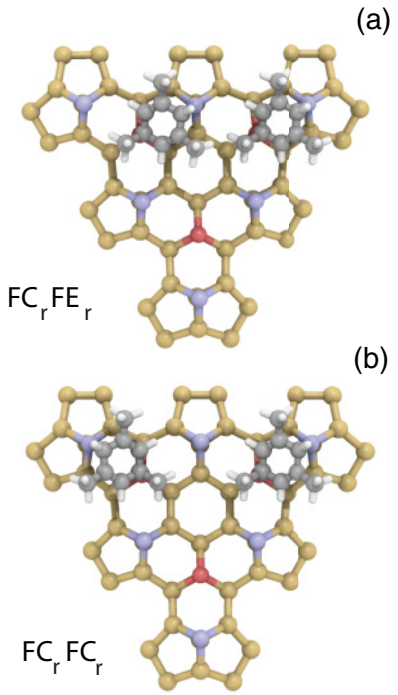

FIG. 9. (Color online) Two mesitylene molecules per 7 × 7 cell in the (a) FC_rFE_r and (b) FC_rFC_r geometries.

Consistent with our results for single-molecule adsorption we found that all adsorption structures that included a molecule in the *a* configuration (e.g., C_a and E_a) were unstable. See, for example, the results for FE_rFC_a and UC_rFC_a listed in Table III. We conclude that for the coverage of two mesitylene molecules per 7 × 7 surface unit cell, the most stable adsorption geometry is the one where the molecules adsorb on the corner sites in the C_rC_r configuration.

Increasing the number of mesitylene molecules further, to the saturation coverage of one molecule per rest atom or equivalently six molecules per 7 × 7 cell, gives rise to a number of array structures that we have examined in detail. However, here we present only the results for three different array configurations, $6C_r$, $5C_rC_a$, and $6E_r$, to illustrate the general trends that were noted (Table IV). There array structures are illustrated in Figs. 10 and 11. The notation $5C_rC_a$ is used to represent the modified corner array comprising three molecules in UC_r sites, two molecules in FC_r sites and one molecule in a FC_a site. In $6C_r$, each molecule acquires the C_r conformation and a schematic rendering of this array is presented in Figs. 10(a) and 10(b). In $5C_rC_a$ one

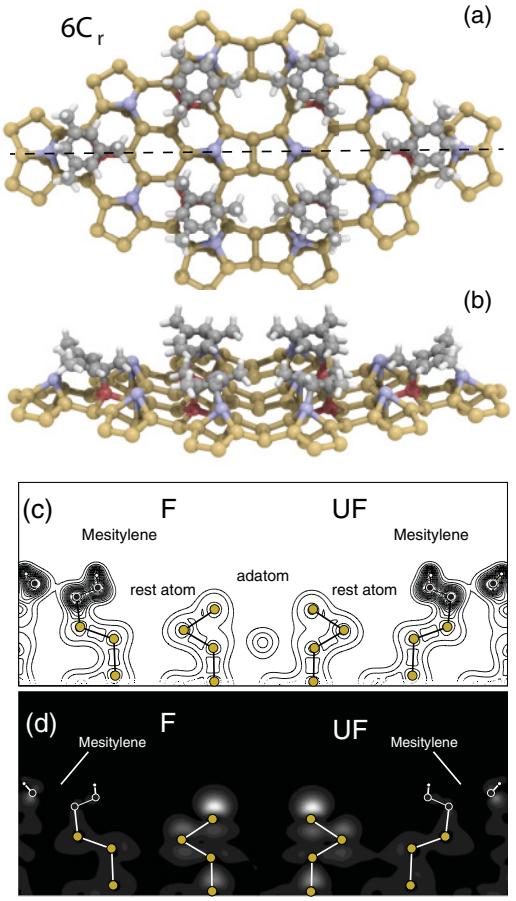

FIG. 10. (Color online) Equilibrium geometry of the $6C_r$ structure: (a) top view; (b) side view. (c) Total change density and (d) partial charge density within E_F–0.8 eV, passing through the mirror symmetry plane the location of which is indicated by a dashed line in panel (a).

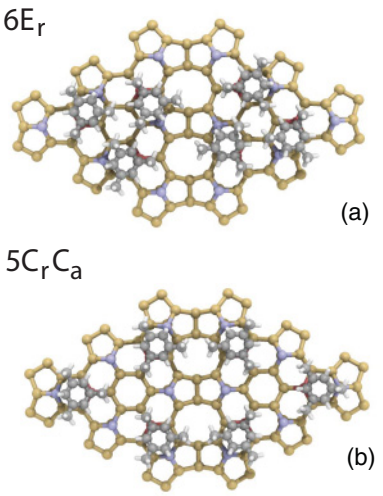

FIG. 11. (Color online) Equilibrium geometry of (a) the 6E_r edge array and (b) the modified corner array 5C_rC_a. Although the edge array is geometrically admissible, it is less stable by 0.224 eV/molecule than the 6C_r array and therefore not favored in thermodynamic equilibrium; three molecules in E_r sites in each half cell are sterically hindered. The modified corner array has one molecule rotated by 60° from C_r to C_a (see the text).

mesitylene molecule is rotated by 60° from the C_r into the C_a geometry. We have already seen that the C_a configuration is not energetically favorable. Consequently, 5C_rC_a is less stable than 6C_r by 81 meV. Additionally, our total energy results indicate that in 6C_r, the molecules are more tightly bound, by 19 meV/molecule, to the surface when compared with a single molecule in the UE_r configuration (the most stable adsorption geometry for a single-molecule/7 × 7 cell).

In the 6C_r structure, the Si adatoms situated at the corner of the HUC and all rest atoms form covalent bonds with the adsorbed molecules, whereas the six Si adatoms situated in the edge positions do not. Moreover, the C-Si bond lengths (≈2.03 Å) for 6C_r are the same as those obtained for the single-molecule geometries considered earlier. Figure 10(c) presents the total charge density along the mirror symmetry plane, indicated by the dashed line in Fig. 10(a), where the covalent character of C-Si bonds is clearly visible. We also find that the molecular structure, at least as ascertained from the total charge density, is preserved upon adsorption. The charge density of 6C_r is shown in Fig. 10(c). However,

TABLE IV. Calculated adsorption energies E_{ads} for a saturation coverage of six molecules per 7 × 7 cell in units of eV/molecule for three different array geometries. In Array 6C_r (Array 6E_r), the molecules bridge a rest atom and a corner (edge) adatom. The second array is a modified version of the first array (see the text), where a molecule in the faulted half cell is rotated by 60°.

Array geometry	E_{ads}
6C_r	0.706
5C_rC_a	0.625
6E_r	0.482

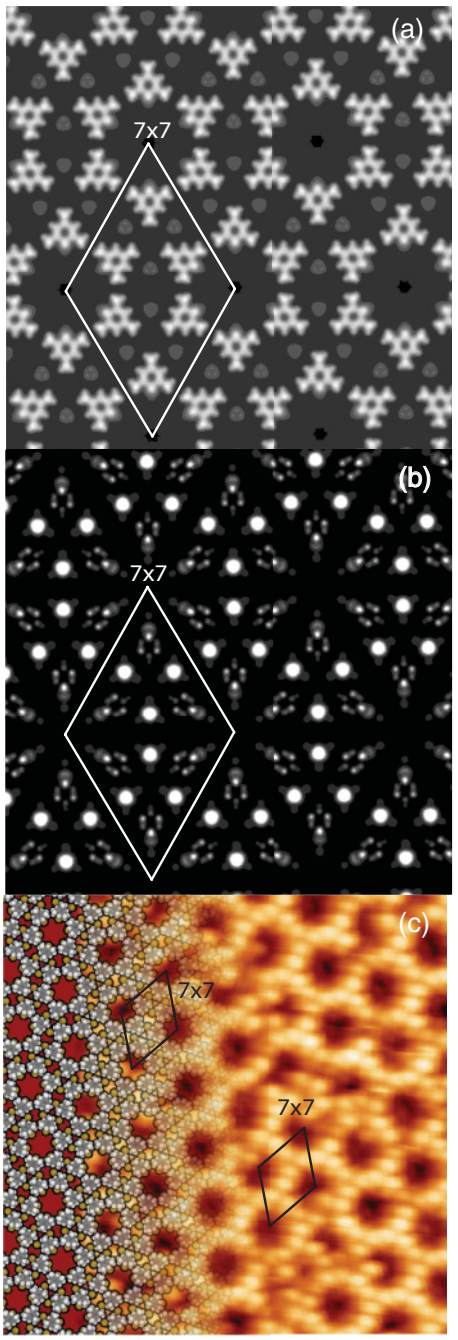

FIG. 12. (Color online) (a) Total charge density and (b) a simulated occupied state STM image within the energy range E_F–0.8 eV for 6C_r. The simulated image is dominated by 12 Si adatom rings visible in the experimental images (c). The weaker features localized on the molecules are due to the C-C bonds within mesitylene's C_6 ring and the corner Si adatom. The side of the 7 × 7 unit cell is 2.7 nm. For comparison with (b), an STM image collected at saturation with a mesitylene corner array overlay to show the close correspondence between the proposed model for the array and the experimental image. Image details: size = 19 × 19 nm, $V_{bias} = -0.8$ V, $I = 0.6$ nA.

similar to all other mesitylene/7 × 7 adsorption geometries we have studied, the occupied electronic states of the adsorbed mesitylene molecule are resonant with the valence band, and therefore invisible within the energy range E_F-0.8 eV. Most of the occupied electronic states are localized on the edge

Si adatoms [Fig. 10(d)]. Indeed, our STM simulation shown in Fig. 12(b) indicates the formation of six bright spots per 7×7 surface unit cell, lying on the edge Si adatoms. This compares favorably with the experimental STM topographic image presented in Fig. 12(c) lending support to the $6C_r$ structure introduced above.

3. *Kinetic Monte Carlo*

The total energy calculations, presented above, allowed us to identify the preferred array geometry in thermodynamic equilibrium. In this section we explore, using the KMC approach, how the molecules assemble into the thermodynamically preferred structure as they are progressively added to the surface.

Before chemisorbing, small organic molecules move freely on 7×7, occupying a mobile precursor state.[35,40] To form covalent bonds with the active binding sites they must surmount an activation energy barrier associated with the distortion of both the surface and the molecule (see above).[49] Previously, we were able to reproduce the experimental site-dependent coverage curves for thiophene using a KMC model with site-dependent activation energies.[34] However, to reproduce the experimental coverage curves for mesitylene, the activation energies had also to depend on the presence of molecules in nearest-neighbor sites. A nearest-neighbor site is one which involves an adatom (rest atom) which is adjacent to the rest atom (adatom) of a given site. The site-dependant activation energies were increased by an additional energy E_{nn} for each such site which was occupied to account for a steric hindrance between mesitylene molecules brought into close proximity. This is consonant with the *ab initio* calculations presented above that provide evidence for nearest-neighbor steric interaction. There are more nearest-neighbor sites for edge than corner sites, so this increase in activation energy makes edge sites less favorable at high surface coverages.

The output of our KMC model is presented in Fig. 13 together with the results of our STM studies. In the simulation, molecules were deposited on the 7×7 surface up to a discrete coverage, after which the simulation progressed for a further time τ at fixed coverage in order to recreate the time that would elapse before experimental observation. During this time of typically 10 min, detachment events, which describe chemisorbed molecules returning to a mobile physisorbed state, must be accounted for. While these events occur at much lower rates than chemisorption events, they allow mesitylene to resample unoccupied chemisorption sites increasing the occupancy of corner sites at high coverages. It was necessary to include this time interval τ in the simulation to achieve agreement with STM data.

The following parameters of the KMC model were varied to minimize the squared difference between the simulated results and experimental observations: the activation energy barriers E_E and E_C for edge and corner sites, the nearest-neighbor repulsive energy E_{nn}, and the detachment frequency ν_d with which molecules reconfigure themselves during the relaxation procedure. Because the STM experiments [Fig. 3(g)] demonstrate that there is no preference for either unit cell half, the activation energies are considered to be symmetric for faulted/unfaulted half cells in the simulation. The results from

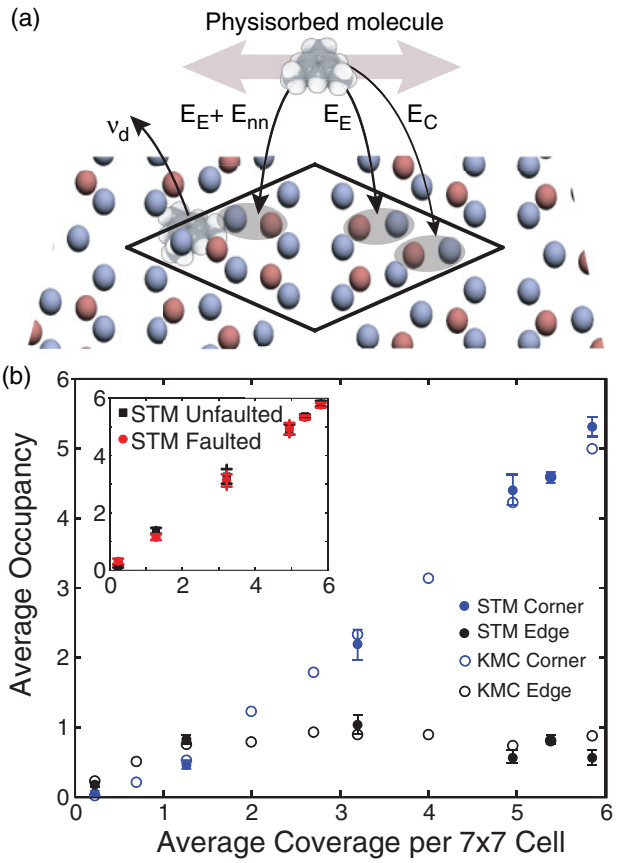

FIG. 13. (Color online) (a) At room temperature, physisorbed molecules are mobile. The activation energy barriers for corner and edge bridging sites are E_C and E_E, respectively. The nearest-neighbor interaction energy is E_{nn}. The desorption rate for chemisorbed molecules is ν_d. (b) The site occupancy as a function of mesitylene coverage was extracted from STM images at different mesitylene coverages. At the two lowest coverages, the molecules show a preference for the edge sites, whereas at all higher coverages the site preference switches to corner. At the saturation coverage, the average occupancy of corner sites is ≈92% of the saturation coverage and the average occupancy of edge sites is 8%. The KMC model (open circles), with parameters $E_E = 0.12$ eV, $E_C = 0.17$ eV, $E_{nn} = 0.11$ eV, $\nu_d = 1$ Hz, is in excellent agreement with STM data (solid blue and black circles) at all coverages. The STM data (inset) reveals that the faulted/unfaulted half-cell occupancy is equal, independent of coverage.

the KMC model are shown in Fig. 13 as blue (corner) and black (edge) open circles. The fixed coverage simulation time τ is 60 s and the temperature is 300 K. The model, which will be described in more detail in a future presentation,[50] is able to successfully explain the crossover in site occupancy and the preference for corner sites at saturation.

III. CONCLUSIONS AND DISCUSSION

We have demonstrated that it is possible to use the Si(111)-7×7 surface reconstruction to template an epitaxial organic layer *in vacuo* without passivating the surface before adsorption. Our strategy is to use steric hindrance to minimize the disorder that arises from the multiplicity of covalent di-σ

bridging geometries. We illustrate this approach using 1,3,5-methyl benzene (mesitylene), chosen because the addition of methyl groups to benzene has been shown to increase the preference for corner adatom attachment.[23] Using STM, total energy calculations, and a KMC model, we demonstrate that the steric interaction caused by the hydrogen atoms in the three methyl groups favors the self-assembly of an ordered corner array, near saturation coverage, because the corner array minimizes the steric interaction energy. The KMC model faithfully reproduces the switch in site preference from edge to corner, observed with STM, as the coverage is increased. The total energy calculations also show that, because of interaction between the methyl groups and the Si adatoms, only one of the two symmetrically distinct attachment geometries (r) is stable at room temperature. This interaction with the surface is an important part of the array ordering process because it eliminates a potential source of disorder.

Will it be possible to extend the approach presented in this paper to other molecules and create alternate arrays? It is important to realize that the steric interaction does not occur in isolation but in the context of chemisorption. Consequently, both the attachment mechanism and the steric interaction must be considered concurrently. The covalent attachment of the molecule to the surface defines the location of the molecular skeleton. The size of the steric interaction (in the case of the molecule considered here) depends upon the relative position of the hydrogen atoms in two adjacent methyl groups. Consequently, the restrictions this places on the molecule are strict. Nevertheless, the understanding of steric interactions is well developed in both chemistry and biochemistry.[51,52] Furthermore, recent wet-chemical studies performed on Si(111)[53] have shown that ordered arrays of methyl groups assemble due to the repulsive interaction between hydrogen atoms on neighboring methyl groups. Wet-chemical templating strategies, which use ordered patterns of methoxy groups, have also recently been developed for Si(111), and these employ steric interactions to modify surface reactions[54] producing nanopatterned organic layers. Drawing upon this wealth of experience, it should be possible to design alternate arrays on 7×7. Furthermore, in the C_6 arrays, described above, there are six Si adatoms/7×7 cell that *do not* form chemical bonds with the organic layer. This suggests the possibility of multicomponent organic overlayers.

ACKNOWLEDGMENTS

We acknowledge financial support from CNPq, FAPEMIG (Brazil), and NSERC (Canada) and computational support from CENAPAD/SP (Brazil). Figures 3, 4, 12, and 13 are reproduced by permission of The Royal Society of Chemistry (Ref. 25).

*Current address: Institute of Experimental and Applied Physics, University of Regensburg, Universitätsstraße 31, D-93053 Regensburg, Germany.

†Corresponding author: mclean@physics.queensu.ca

[1] J. Heath, Annu. Rev. Mater. Res. **39**, 1 (2009).
[2] A. Vilan, O. Yaffe, A. Biller, A. Salomon, A. Kahn, and D. Cahen, Adv. Mater. **22**, 140 (2010).
[3] N. Lin, S. Stepanow, M. Ruben, and J. V. Barth, Top. Curr. Chem. **287**, 1 (2009).
[4] J. V. Barth, Surf. Sci. **603**, 1533 (2009).
[5] R. Hamers, Annu. Rev. Anal. Chem. **1**, 707 (2008).
[6] R. Wolkow, Annu. Rev. Phys. Chem. **50**, 413 (1999).
[7] M. A. Filler and S. F. Bent, Prog. Surf. Sci. **73**, 1 (2003).
[8] T. R. Leftwich and A. V. Teplyakov, Surf. Sci. Rep. **63**, 71 (2008).
[9] J. M. Buriak, Chem. Rev. **102**, 1271 (2002).
[10] S. Bent, Surf. Sci. **500**, 879 (2002).
[11] R. Hamers, J. Hovis, S. Lee, H. Liu, and J. Shan, J. Phys. Chem. B **101**, 1489 (1997).
[12] I. R. Mcnab and J. Polanyi, Chem. Rev. **106**, 4321 (2006).
[13] P. Guaino, D. Carty, G. Hughes, P. Moriarty, and A. A. Cafolla, Appl. Surf. Sci. **212**, 537 (2003).
[14] J. A. Theobald, N. S. Oxtoby, M. A. Phillips, N. R. Champness, and P. H. Beton, Nature (London) **424**, 1029 (2003).
[15] R. J. Hamers, S. K. Coulter, M. D. Ellison, J. S. Hovis, D. F. Padowitz, and M. P. Schwartz, Acc. Chem. Res. **33**, 617 (2000).
[16] P. Guaino, A. A. Cafolla, D. Carty, G. Sheerin, and G. Hughes, Surf. Sci. **540**, 107 (2003).
[17] S. Dobrin, X. Lu, F. Naumkin, J. Polanyi, and J. Yang, Surf. Sci. **573**, L363 (2004).
[18] Y. Makoudi, M. Arab, F. Palmino, É. Duverger, C. Ramseyer, F. Picaud, and F. Chérioux, Angew. Chem. Int. Edit. **46**, 9287 (2007).
[19] Y. Makoudi, M. Garah, F. Palmino, E. Duverger, and M. Arab, Surf. Sci. **602**, 2719 (2008).
[20] M. E. Garah, Y. Makoudi, É. Duverger, F. Palmino, A. Rochefort, and F. Chérioux, ACS Nano **5**, 424 (2011).
[21] Z. Wang, Y. Cao, and G. Xu, Chem. Phys. Lett. **338**, 7 (2001).
[22] X. Lu, X. Wang, Q. Yuan, and Q. Zhang, J. Am. Chem. Soc. **125**, 7923 (2003).
[23] H. Tomimoto, T. Sekitani, R. Sumii, E. O. Sako, S. Wada, and K. Tanaka, Surf. Sci. **566**, 664 (2004).
[24] K. D. Brommer, M. Galvan, A. DalPino, and J. D. Joannopoulos, Surf. Sci. **314**, 57 (1994).
[25] A. J. Weymouth, R. H. Miwa, G. J. A. Edge, G. P. Srivastava, and A. B. McLean, Chem. Commun. **47**, 8031 (2011).
[26] P. Hohenberg and W. Kohn, Phys. Rev. **136**, B864 (1964).
[27] J. P. Perdew, K. Burke, and M. Ernzerhof, Phys. Rev. Lett. **77**, 3865 (1996).
[28] N. Troullier and J. Martins, Phys. Rev. B **43**, 1993 (1991).
[29] L. Kleinman and D. M. Bylander, Phys. Rev. Lett. **48**, 1425 (1982).
[30] O. F. Sankey and D. J. Niklewski, Phys. Rev. B **40**, 3979 (1989).
[31] E. Artacho, D. Sánchez-Portal, P. Ordejón, A. Garcia, and J. M. Soler, Status Solid B **215**, 809 (1999).
[32] J. M. Soler, E. Artacho, J. D. Gale, A. García, J. Junquera, P. Ordejón, and D. Sánchez-Portal, J. Phys. Condens. Matter **14**, 2745 (2002).
[33] S. Grimme, J. Comput. Chem. **27**, 1787 (2011).

[34]A. J. Weymouth, R. H. Miwa, G. P. Srivastava, and A. B. McLean, Phys. Status Solidi C **7**, 240 (2010).
[35]D. E. Brown, D. J. Moffatt, and R. A. Wolkow, Science **279**, 542 (1998).
[36]P. Sobotík, P. Kócan, and I. Ošt'ádal, Surf. Sci. **537**, L442 (2003).
[37]R. A. Wolkow and D. J. Moffatt, J. Chem. Phys. **103**, 10696 (1995).
[38]Y. Cao, X. M. Wei, W. S. Chin, Y. H. Lai, J. F. Deng, S. L. Bernasek, and G. Q. Xu, J. Phys. Chem. B **103**, 5698 (1999).
[39]Z. Wang, Y. Cao, and G. Q. Xu, Chem. Phys. Lett. **338**, 7 (2001).
[40]M. Carbone, M. N. Piancastelli, M. P. Casaletto, R. Zanoni, M. J. Besnard-Ramage, G. Comtet, G. Dujardin, and L. Hellner, J. Phys. Condens. Matter **15**, L327 (2003).
[41]H. Tomimoto, Surf. Sci. **566-568**, 664 (2004).
[42]Y. Cao, K. S. Yong, Z. Q. Wang, W. S. Chin, Y. H. Lai, J. F. Deng, and G. Q. Xu, J. Am. Chem. Soc. **122**, 1812 (2000).
[43]Y. Cao, K. S. Yong, Z. H. Wang, J. F. Deng, Y. H. Lai, and G. Q. Xu, J. Chem. Phys. **115**, 3287 (2001).
[44]R. H. Miwa, A. J. Weymouth, A. B. McLean, and G. P. Srivastava, Phys. Rev. B **80**, 115317 (2009).
[45]S. F. Boys and F. Bernardi, Mol. Phys. **19**, 553 (1970).
[46]C. Hobbs, K. Kantorovich, and J. D. Gale, Surf. Sci. **591**, 45 (2005).
[47]J. Tersoff and D. R. Hamann, Phys. Rev. B **31**, 805 (1985).
[48]S. A. Horn and S. N. Patitsas, Surf. Sci. **602**, 630 (2008).
[49]X. Lu, X. L. Wang, Q. H. Yuan, and Q. Zhang, J. Am. Chem. Soc. **125**, 7923 (2003).
[50]G. J. A. Edge, A. J. Weymouth, A. B. McLean, R. H. Miwa, and G. P. Srivastava (to be published).
[51]H. Förster and F. Vögtle, Angew. Chem., Int. Ed. Engl. **16**, 429 (1977).
[52]J. K. Badenhoop and F. Weinhold, J. Chem. Phys. **107**, 5406 (1997).
[53]H. Yu, L. J. Webb, R. S. Ries, S. D. Solares, W. A. G. III, J. R. Heath, and N. S. Lewis, J. Phys. Chem. B **109**, 671 (2005).
[54]D. J. Michalak, S. R. Amy, D. Aureau, M. Dai, A. Estève, and Y. J. Chabal, Nat. Mater. **9**, 266 (2010).